Charge Transfer in Covalently-Linked Porphyrin–Donor Complexes from Picosecond Transient Absorption Spectroscopy

Glen R. Loppnow, Dan Melamed,† Andrew D. Hamilton,‡ and Thomas G. Spiro*

Department of Chemistry, Princeton University, Princeton, New Jersey 08544

Received: March 10, 1993; In Final Form: May 20, 1993

Octaalkyl free base porphyrins have been synthesized with covalently attached electron donors at a single *meso* position. Singlet-state lifetimes were determined from fluorescence quenching in three solvents and were found to be ≤1.5 ps for the *N,N,N′,N′*-tetramethyl-1,4-phenylenediamine (TMPD) appended complex, 1.3 ns for the phenyl–TMPD-appended complex, and ≥5 ns for the phenyl-appended, *N,N*-dimethylaniline (DMA) appended, and DMA–TMPD-appended porphyrin complexes in *o*-difluorobenzene. Single photon counting measurements and fluorescence quantum yield quenching studies of the phenyl-appended control and phenyl-TMPD charge-transfer complex gave 14 ± 3 and 2 ± 0.3 ns excited-state lifetimes, respectively. Fluorescence quantum yields of the TMPD and phenyl–TMPD porphyrins were higher in solvents with lower dielectric constants. Picosecond absorption spectroscopy was performed on molecules exhibiting fluorescence quenching to characterize the charge-transfer state and to determine the recombination kinetics. Conclusive evidence of charge transfer was obtained by observing the donor cation absorption at 606 nm for the TMPD and phenyl–TMPD porphyrins. Picosecond absorption changes in the 380–500-nm region are complete within 50 ps for the TMPD-appended free base porphyrin and 11.5 ns for the phenyl–TMPD-appended free base porphyrin. First-order kinetic analysis indicates that the charge recombination rates are 26 ± 3 ps and 3.5 ± 0.4 ns for the TMPD-appended and phenyl-TMPD-appended complexes, respectively. These data yield β = 0.8–1.1 Å^{-1} for the exponent in the distance dependence of the electron-transfer rate, $\exp\{-\beta(r - r_0)\}$. Inasmuch as similar β values have been determined for electron transfer through saturated bonds, it can be concluded that the π system of the *meso* substituents is ineffective in mediating electron transfer, as expected from the near orthogonality of the porphyrin and substituent rings. This is the first systematic study of electron transfer in porphyrin–donor complexes.

Introduction

Porphyrins play a key role in both natural and synthetic electron-transfer systems. Many biological electron transfers are mediated by porphyrin-containing cytochromes,[1] and the photosynthetic reaction centers of bacteria[2] and plants[3] utilize hydroporphyrins in the electron-transfer cascade. The advantageous photophysical and electrochemical characteristics of porphyrins have been exploited to study the factors governing the mechanisms of electron transfer, primarily by using model porphyrins with covalently-linked donor or acceptor substituents.[4]

Much of this research has involved porphyrins covalently linked to electron acceptors, to mimic the final electron-transfer step in bacterial photosynthetic reaction centers. For example, a carotene–porphyrin–porphyrin–benzoquinone tetrad has been characterized in an effort to mimic both the energy-transfer and electron-transfer processes in bacterial photosynthetic reaction centers.[5] Wasielewski et al. have studied a variety of porphyrin–quinone systems with fluorescence lifetime measurements and transient absorption spectroscopy to show that electron transfer can occur in these systems in times as fast as 5 ps.[6-9] Joran et al. have used quinones appended to octaalkylporphyrins through phenyl–bicyclooctane spacers to examine the effects of distance on charge separation rates.[10] Recently, Harriman et al. have used a quinone bound to a porphyrin through a purine–pyrimidine hydrogen bond to approximate the noncovalent association of the chromophores in the reaction center.[11] They were able to see electron transfer on a 3-ns time scale, consistent with the bacteriopheophytin → quinone electron transfer in the photosynthetic reaction center. Porphyrin–quinone systems have also been used to examine the orientation dependence, bridge dependence, and solvent dependence of electron-transfer rates.[12-14] Additional donor groups have been incorporated in these systems, in order to study multistep electron-transfer cascades.

Surprisingly few studies, however, have examined single electron transfer *to* a porphyrin from an attached donor. Harriman and Hosie reported the synthesis and fluorescence quenching of *meso*-tetrasubstituted [*p*-(*N,N*-dimethylamino)-phenyl]- and (2,5-dihydroxyphenyl)porphyrin free bases.[15] The magnitude of fluorescence quenching for these porphyrins was relatively small (~5×), probably as a result of the solvent chosen and relatively low electrochemical driving force. In a study of a zinc porphyrin covalently linked to both a donor and acceptor, Wasielewski et al. have determined that the electron transfer occurs from the excited state of the zinc porphyrin to the naphthoquinone acceptor on a ~10-ps time scale, and subsequently an electron is transferred from the covalently-linked *N,N,N′,N′*-tetraalkyl-*p*-phenylenediamine donor to the oxidized porphyrin on a ~500-ps time scale.[16]

In this study, electrochemistry, picosecond transient absorption spectroscopy, and fluorescence lifetime measurements are applied to the characterization of the excited-state properties of novel porphyrin complexes having a single *meso*-substituted electron donor. The substituent was varied systematically from a phenyl, to an *N,N*-dimethylaniline (DMA), to an *N,N,N′,N′*-tetramethyl-1,4-phenylenediamine (TMPD), to a phenyl-linked TMPD, and to a DMA-linked TMPD (Scheme I). Charge transfer is indicated by fluorescence quenching and picosecond transient absorption spectroscopy in the TMPD-appended and the phenyl–TMPD-appended porphyrins. No significant fluorescence quenching is seen for the DMA–TMPD- or DMA-appended porphyrins, consistent with the electrochemical observation of a charge-transfer state higher than the lowest-lying singlet excited state. Picosecond transient absorption spectroscopy establishes charge recombination on time scales of 26 ps and 3.5 ns for the TMPD-

* To whom correspondence should be addressed.
† Present address: Department of Chemistry, University of Texas, Austin, TX 78712.
‡ Present address: Department of Chemistry, University of Pittsburgh, Pittsburgh, PA 15260.

0022-3654/93/2097-8957$04.00/0

SCHEME I

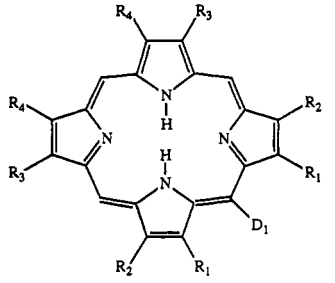

Porphyrin	R_1	R_2	R_3	R_4	D_1
HEDM-P	Et	Et	Me	Et	
TETM-A	Me	Et	Me	Et	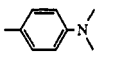
HEDM-T	Et	Et	Me	Et	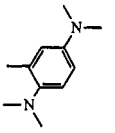
HEDM-PT	Et	Et	Me	Et	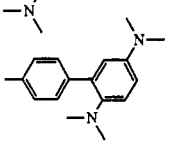
TETM-AT	Et	Me	Me	Et	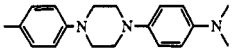

appended and phenyl–TMPD-appended porphyrins, respectively. The charge separation and recombination rates are comparable to those observed in acceptor-appended porphyrins. These results are discussed in terms of the Marcus theory of electron transfer.

Materials and Methods

Synthesis of Porphyrin–TMPD Complexes. All chemicals were obtained from Aldrich Chemical Co. and used as received, unless otherwise specified. Tetrahydrofuran (THF) was distilled over lithium aluminum hydride immediately before use. *N,N*-Dimethylformamide (DMF) was distilled over barium oxide under reduced pressure and stored over molecular sieves. NMR measurements were taken on a General Electric 300-MHz or a JEOL 270-MHz NMR spectrometer. A Kratos MS50 RFA high-resolution mass spectrometer was utilized for all mass spectroscopic measurements. Syntheses of the porphyrin–donor complexes shown in Scheme I are shown in Schemes II and III and are described in detail below.

2,5-(N,N,N',N'-Tetramethyldiamino)benzaldehyde. 1,4-(*N,N,N',N'*-Tetramethyldiamino)benzene (7.8 g, 0.05 mol) in 100 mL of dry hexanes was refluxed with *n*-butyl lithium (20 mL of a 2.5 M solution in hexanes, 0.05 mol) under nitrogen during which a yellow precipitate was observed. After cooling, the hexanes were decanted and the precipitate was redissolved in 100 mL of freshly distilled THF. *N*-formylmorpholine (5 mL, 0.05 mol) in 15 mL of THF was added dropwise over 15 min and stirred for 8 h. After evaporation of the solvent, the residue was dissolved in 50 mL of 10% HCl. After 15 min, the solution was neutralized with sodium hydroxide and extracted with dichloromethane. Water was removed from the extracted solution with sodium sulfate, and the solvent was removed under vacuum. Chromatography on silica gel with dichloromethane as eluant yielded 2.62 g (0.014 mol, 27% yield) as a red brown oil. NMR ($CDCl_3$) (ppm): δ 2.79 (s, 6H, $N(CH_3)_2$), 2.93 (s, 6H, $N(CH_3)_2$ ortho to the formyl group), 6.96 (dd, J = 9.00 Hz, J' = 2.98 Hz, 1 H), 7.08 (d, J = 9.00 Hz, 1 H), 7.16 (d, J = 2.98 Hz, 1 H), 10.41 (s, 1 H, formyl). Calculated mass 192.1258; found 192.1259 (M^+).

[2,5-(N,N,N',N'-Tetramethyldiamino)phenyl]zinc Chloride. *n*-Butyl lithium (20 mL of a 2.5 M solution in hexanes, 0.05 mol) was added to 1,4-(*N,N,N',N'*-tetramethyldiamino)benzene (7.8 g, 0.05 mol) in 100 mL of dry hexanes under nitrogen and refluxed for 48 h during which a yellow precipitate was observed. After 48 h, the hexanes were decanted and 50 mL of freshly distilled THF was added. Zinc chloride (30 mL of a 0.1 M solution, 3 mmol) was added, and the solution was stirred for 30 min. The compound was used without further isolation or purification.

4-[2',5'-(N,N,N',N'-Tetramethyldiamino)biphenyl]benzonitrile. Nickel tris(acetylacetonate) (0.32 g, 1.25 mmol) was mixed with triphenylphosphine (1.31 g, 5 mmol), 15 mL of THF, and diisobutylaluminum hydride (DIBAL) (1.0 mL of a 1 M solution, 1 mmol). After the solution turned from green to red, 4-bromobenzonitrile (3.6 g, 20 mmol) was added. [2,5-(*N,N,N',N'*-Tetramethyldiamino)phenyl]zinc chloride was transferred with a canula into the solution, and the reaction mixture was stirred for 8 h. The solvent was evaporated under vacuum, the residue was redissolved in dichloromethane, and the solution was filtered through alumina. Chromatography on silica gel with dichloromethane as eluant yielded 1.2 g (4.5 mmol, 21% yield) as a yellow solid (mp 53.5–54.5 °C). NMR (CD_3CN) (ppm): δ 2.87 (s, 6 H, $N(CH_3)_2$), 3.04 (s, 6 H, $N(CH_3)_2$, ortho to the biaryl bond), 7.45 (d, J = 1.32 Hz, 1 H, ortho to the biaryl bond and the $N(CH_3)_2$), 7.62 (dd, J = 8.58 Hz, J' = 1.98 Hz, 2 H, ortho to the biaryl bond), 7.86 (dd, J = 8.58 Hz, J' = 1.98 Hz, 2 H, ortho to the nitrile), 7.72 (d, J = 1.32 Hz, 2 H, ortho to the $N(CH_3)_2$). Calculated mass 265.1574; found 265.1573 (M^+).

4-[2',5'-(N,N,N',N'-Tetramethyldiamino)biphenyl]benzaldehyde. DIBAL (5 mL of a 0.1 M solution, 0.5 mmol) was added over several minutes to a 0 °C solution of 4-[2',5'-(*N,N,N',N'*-tetramethyldiamino)biphenyl]benzonitrile (0.95 g, 3.6 mmol) in 20 mL of freshly distilled THF under argon. After stirring for 8 h, the mixture was poured into 150 mL of a 10% HCl solution, stirred for 30 min, neutralized with potassium carbonate, and filtered. The precipitate was dissolved in methanol, filtered, and evaporated under vacuum to yield 0.66 g (2.5 mmol, 69% yield) as a yellow oil. NMR ($CDCl_3$) (ppm): δ 2.45 (s, 6 H, NMe_2), 2.90 (s, 6 H, NMe_2, ortho to the biaryl bond), 6.66 (d, J = 2.96 Hz, 1 H, ortho to the biaryl bond and the NMe_2), 6.73 (dd, J = 2.96 Hz, J' = 8.91 Hz, 1 H), 7.04 (d, J = 8.91 Hz, 1 H), 7.74 (dd, J = 6.6 Hz, J' = 1.65 Hz, 2 H, ortho to the biaryl bond), 7.87 (dd, J = 6.60 Hz, J' = 1.98 Hz, 2 H, ortho to the aldehyde), 10.23 (s, 1 H, formyl). Calculated mass 268.1575; found 268.1571 (M^+).

N-Phenyl-N'-(4-nitrophenyl)piperazine. 4-(Fluoronitro)benzene (3 mL, 0.028 mol) and *N*-phenylpiperazine (5 mL, 0.033 mol) were heated at 60 °C in dry *N,N*-dimethylformamide (50 mL). After 3 h, the solution was poured into 50 mL of ice water and neutralized with a saturated sodium carbonate solution. The mixture was filtered and washed with water, and the filtrate was recrystallized from acetone to yield 6.6 g (0.023 mol, 82% yield) as yellow needles (mp 194.5–196 °C). NMR ($CDCl_3$) (ppm): δ 3.36 (4 H, m, piperazine), 3.59 (4 H, m, piperazine), 6.87 (5 H, m, phenyl), 7.30 (2 H, m, phenyl), 8.16 (2 H, d, J = 9.10 Hz, phenyl at C3' and C5'). Calculated mass 283.1321; found 283.1316 (M^+).

N-(4-Formylphenyl)-N'-(4-nitrophenyl)piperazine. Phosphorous oxychloride (1.5 mL, 16 mmol) was added dropwise to 50 mL of dry, ice-cold *N,N*-dimethylformamide. *N*-Phenyl-*N'*-(4-nitrophenyl)piperazine (3 g, 11 mmol) was added, and the mixture was heated to 60 °C. After 2 h, the solution was poured into 50 mL of ice water and neutralized with a saturated sodium carbonate solution. Filtration and recrystallization from acetone afforded 2.2 g (7 mmol, 64% yield) of brown needles (mp 199.5–201.5 °C). NMR ($CDCl_3$) (ppm): δ 3.66 (8 H, m, piperazine), 6.83 (2 H, d, J = 9.30 Hz, phenyl at C2 and C6), 6.92 (2H, d, J = 8.80 Hz, phenyl at C'2 and C'6), 7.80 (2 H, d, J = 8.80 Hz,

SCHEME II

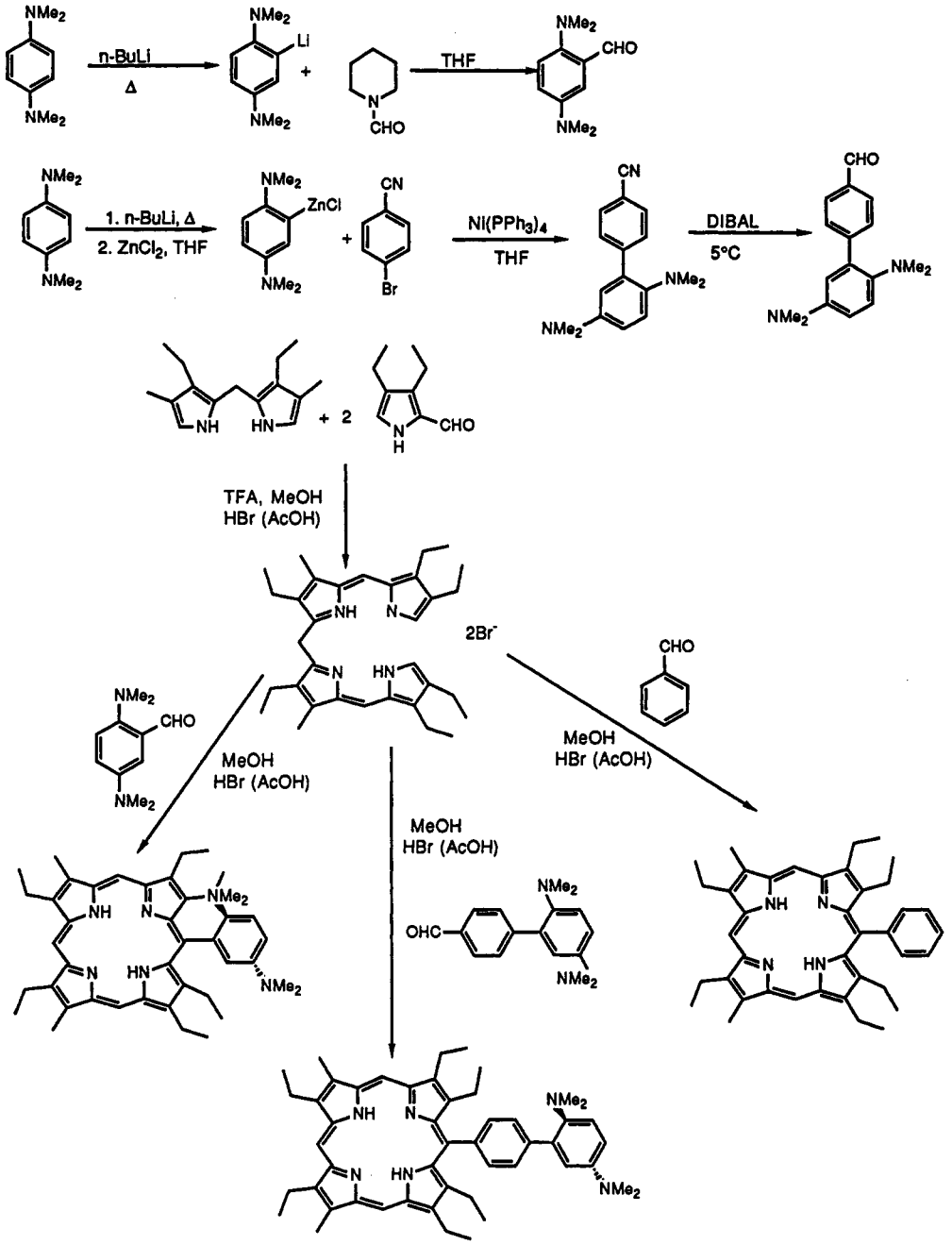

phenyl at C3 and C5), 8.16 (2 H, d, J = 9.30 Hz, phenyl at C'3 and C'5). Calculated mass 311.1270; found 311.1245 (M^+).

Bis{5-(ethoxycarbonyl)-3-ethyl-4-methyl-2-pyrryl}(N-phenyl-N'-(4'-(dimethylamino)phenyl)piperazinyl)methane. Ethyl 4-ethyl-3-methylpyrrole-2-carboxylate (4.19 g, 23.1 mmol), *N*-(4-formylphenyl)-*N'*-(4-nitrophenyl)piperazine (3.6 g, 12 mmol), and 1 mL of concentrated hydrochloric acid were refluxed in 150 mL of ethanol under argon for 3 h. After removal of the ethanol under reduced pressure, the residue was redissolved in 300 mL of acetic acid and filtered through Raney nickel. Formaldehyde (3 mL of a 36% aqueous solution, 40 mmol) and 10% palladium on carbon (250 mg) were added, and the mixture was shaken under 30 psi of hydrogen for 8 h. The solution was filtered through celite, and the solvent was removed under reduced pressure. The residue was redissolved in dichloromethane and neutralized with saturated sodium bicarbonate. The dichloromethane phase was dried and filtered, and the solvent was evaporated under reduced pressure. Chromatography on alumina with dichloromethane as eluant yielded 2.46 g (9.26 mmol, 84.0% yield) of a yellow oil. NMR ($CDCl_3$) (ppm): δ 0.87 (t, 6 H, J = 7.47 Hz, CH_2CH_3), 1.29 (t, 6 H, J = 7.25, OCH_2CH_3), 2.28 (s, 6 H, pyrrole CH_3), 2.89 ppm (m, 10 H, $N(CH_3)_2$ and pyrrole CH_2CH_3), 3.19 (m, 4 H, piperazine), 3.31 (m, 4 H, piperazine), 4.22 (q, J = 7.13 Hz, 4 H, OCH_2CH_3), 5.49 (s, *meso* CH), 6.76 (d, J = 7.1 Hz, 2 H, ortho to the $N(CH_3)_2$), 6.89 (m, 6 H, arene), 8.31 (br s, 2 H, NH). Calculated mass 653.3941; found 653.3869 (M^+).

Bis(3-ethyl-4-methyl-2-pyrryl)(N-phenyl-N'-(4'-(dimethylamino)phenyl)piperazinyl)methane. Bis{5-(ethoxycarbonyl)-3-ethyl-4-methyl-2-pyrryl}(*N*-phenyl-*N'*-(4'-(dimethylamino)phenyl)piperazinyl)methane (2.10 g, 3.21 mmol) was refluxed with 100 mL of ethanol under argon. Sodium hydroxide (15 mL of a 3 N aqueous solution, 45 mmol) was added. After 9 h, glacial acetic acid (3 mL, 52 mmol) was added and filtered, and the precipitate was redissolved in 40 mL of ethanolamine. After refluxing under argon for 6 h, the mixture was cooled, poured over 500 g of crushed ice, and extracted with dichloromethane. The dichloromethane phase was dried with sodium sulfate, and the solvent was removed under reduced pressure to yield 1.26 g (2.47 mmol, 77.2% yield) of a brown powder, (mp 173.5–177.0 °C, dec.). NMR ($CDCl_3$) (ppm): δ 0.90 (t, 6 H, J = 7.45 Hz,

SCHEME III

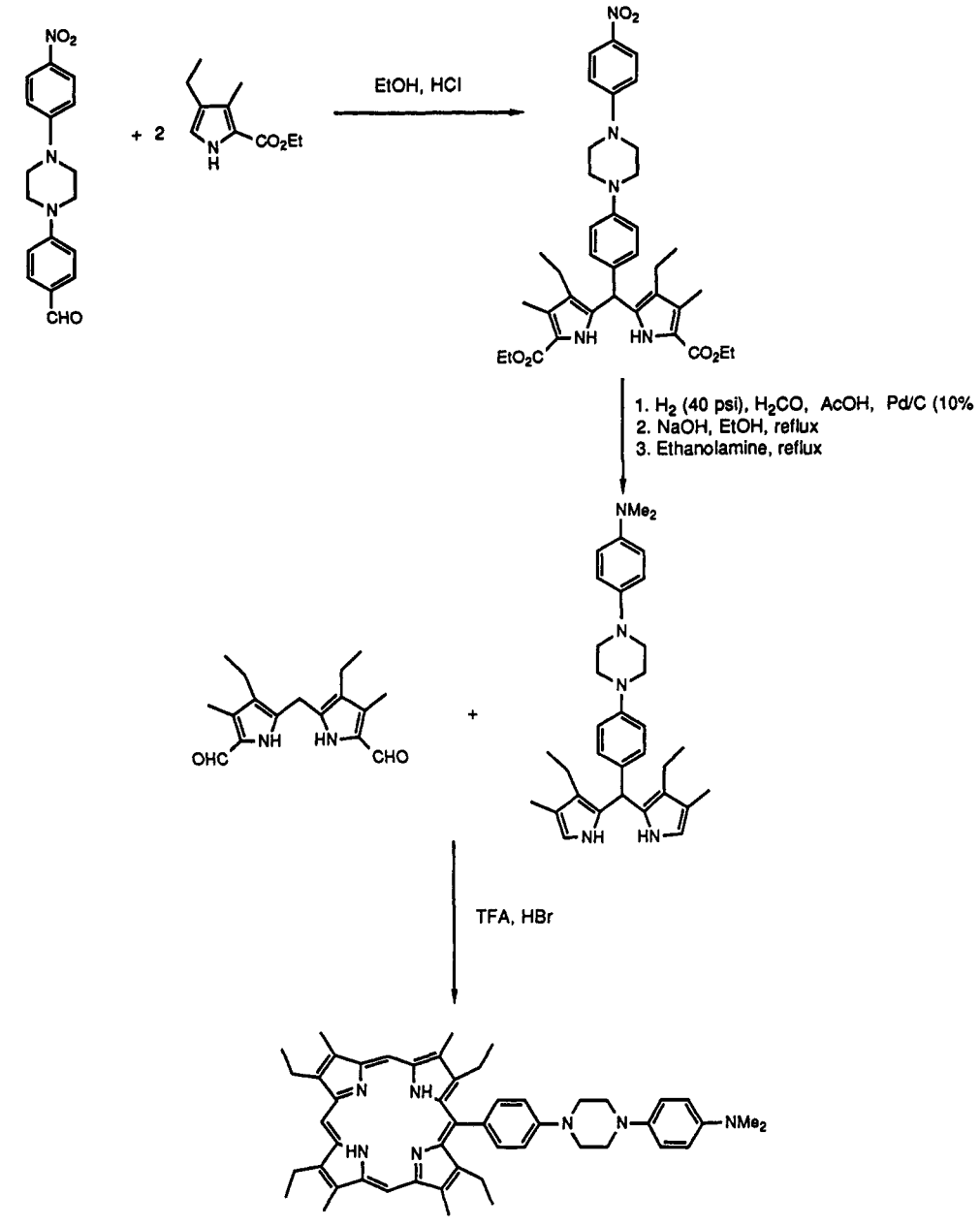

CH_2CH_3), 2.05 (s, 6 H, pyrrole CH_3), 2.27 (q, J = 7.45 Hz, 4 H and pyrrole CH_2CH_3), 2.91 ppm (s, 6 H, $N(CH_3)_2$), 3.24 (m, 4 H, piperazine), 3.32 (m, 4 H, piperazine), 5.47 (s, *meso* CH), 6.36 (d, J = 1.90 Hz, 2 H, pyrrole H), 6.89 (m, phenyl). Calculated mass 509.3518; found 509.3511 (M^+).

1,19-Dideoxy-2,7,13,18-tetraethyl-3,8,12,17-tetramethylbiladiene-ac Dihydrobromide. Bis(4-ethyl-3-methyl-2-pyrryl)-methane (0.25 g, 11 mmol) was mixed in 2 mL of trifluoroacetic acid. Acetic acid saturated with hydrogen bromide (1 mL) was added followed by the slow addition of 2-formyl-3-ethyl-4-methylpyrrole (0.29 g, 21 mmol) dissolved in 1 mL of methanol. After 20 min, 50 mL of dry diethyl ether was slowly added. The solution was filtered, and the precipitate was washed with dry diethyl ether and air-dried to give 0.43 g (mmol, 75.8% yield) of a red powder with a greenish tint. NMR ($CDCl_3$ + TFA-*d*) (ppm): δ 1.0 (t, 6 H, CH_2CH_3), 1.2 (t, 6 H, CH_2CH_3), 2.1 (s, 3 H, CH_3), 2.3 (s, 3 H, CH_3), 2.5 (q, 4 H, CH_2CH_3), 2.6 (q, 4 H, CH_2CH_3), 4.5 (br s, 2 H, *meso* CH_2), 7.3 (s, 2 H, methine CH), 7.7 (d, 2 H, pyrrole).

1,19-Dideoxy-2,3,7,8,13,18-hexaethyl-12,18-dimethylbiladiene-ac dihydrobromide. Bis(5-formyl-4-ethyl-3-methyl-2-pyrryl)methane (0.37 g, 1.5 mmol) was dissolved in 2 mL of trifluoroacetic acid. 3,4-Diethylpyrrole (0.40 mL, 3.3 mmol) was added and the solution was stirred for 8 h. A 50-mL aliquot of dry diethyl ether was added, and the solution was cooled overnight. Filtration yielded a red powder (0.85 g, 89% yield) with a greenish tint (mp > 300 °C). NMR ($CDCl_3$ + TFA-*d*) (ppm): δ 1.08 (t, 6 H, CH_2CH_3), 1.10 (m, 12 H, CH_2CH_3), 2.38 (s, 6 H, CH_3), 2.52 (q, 8 H, CH_2CH_3), 2.6 (q, 4 H, CH_2CH_3), 4.53 (br s, 2 H, meso CH_2), 7.38 (s, 2 H, methine CH), 7.77 (d, 2 H, pyrrole).

1-(2,3,7,8,13,17-Hexaethyl-12,18-dimethylporphyrin-5-yl)-benzene (HEDM-P). Benzaldehyde and 1,19-dideoxy-2,3,8,12,-17,18-hexaethyl-7,13-dimethylbiladiene-ac dihydrobromide were mixed in 35 mL of methanol. Six drops of acetic acid saturated with hydrobromic acid were added, and the mixture was refluxed for 24 h. After cooling, ~150 mL of saturated potassium carbonate solution was added and the solution was extracted with dichloromethane. The dichloromethane phase was dried and evaporated under vacuum. Chromatography on silica gel was accomplished by eluting with a 10:1 dichloromethane/ethyl acetate solution. The resulting compound was purified on three consecutive silica prep plates by elution with a 10:1 dichloromethane/methanol solution and then recrystallized from

methanol/chloroform yielding a red powder. NMR (CD_2Cl_2) (ppm): δ –3.17 (s, 1 H, NH), –3.03 (s, 1 H, NH), 1.145 (m, 6 H, CH_2CH_3, α to the *meso*-arene), 1.604 (m, 12 H, CH_2CH_3), 2.76 (m, 2 H, CH_2CH_3, α to the *meso*-arene), 3.66 (s, 6 H, CH_3), 4.03 (m, 8 H, CH_2CH_3), 7.662 (m, 2 H, arene), 7.809 (m, 1 H, arene), 8.231 (m, 2 H, arene α to the porphyrin), 9.926 (s, 1 H, *meso*) 10.182 (s, 2 H, *meso*). Calculated mass 582.3711; found 582.3709 (M^+).

2,5-(N,N,N',N'-Tetramethyldiamino)-1-(2,3,7,8,13,17-hexaethyl-12,18-dimethylporphyrin-5-yl)benzene (HEDM-T). 1,19-Dideoxy-2,3,8,12,17,18-hexaethyl-7,13-dimethylbiladiene-ac dihydrobromide (170 mg, 0.26 mmol) and 4-[2',5'-(*N,N,N',N'*-tetramethyl diamino)biphenyl]benzaldehyde (0.5 g, 2.6 mmol) were mixed in 35 mL of methanol. Six drops of acetic acid saturated with hydrobromic acid were added, and the mixture was refluxed for 24 h. After cooling, ~150 mL of a saturated potassium carbonate solution was added, and the solution was extracted with dichloromethane. The dichloromethane phase was dried and evaporated under vacuum. Chromatography on silica gel was accomplished by eluting with a 10:1 dichloromethane/ethyl acetate solution. The resulting compound was purified on three consecutive silica prep plates by elution with a 10:1 dichloromethane/methanol solution and then recrystallized from methanol/chloroform yielding a red powder (15 mg, 0.022 mmol, 8.7% yield). NMR (CD_2Cl_2) (ppm): δ –3.17 (s, 1 H, NH), –3.03 (s, 1 H, NH), 1.26 (m, 6 H, CH_2CH_3, α to the *meso*-arene), 1.84 (m, 12 H, CH_2CH_3), 2.086 ppm (s, 6 H, $N(CH_3)_2$, α to the porphyrin), 2.657 (m, 2 H, CH_2CH_3, α to the *meso*-arene), 3.0547 (s, 6 H, $N(CH_3)_2$), 3.1051 (m, 2 H, CH_2CH_3, α to the *meso*-arene), 3.65 (s, 6 H, CH_3), 4.03 (m, 8 H, CH_2CH_3), 7.2018 (dd, J = 2.97 Hz, J' = 8.58 Hz, 1 H), 7.3997 (d, J = 8.58 Hz, 1 H), 7.7086 (d, J = 2.97 Hz, 1 H), 9.936 (s, 1 H, *meso*) 10.163 (s, 1 H, *meso*). Calculated mass 668.45; found 669.4 (M^+).

2',5'-(N,N,N',N'-Tetramethyldiamino)-4-(2,3,7,8,13,17-hexaethyl-12,18-dimethylporphyrin-5-yl)biphenyl (HEDM-PT). 1,19-Dideoxy-4-[2',5'-2,3,8,12,17,18-hexaethyl-7,13-dimethylbiladiene-ac dihydrobromide (110 mg, 0.17 mmol) and 4-[2',5'-(*N,N,N',N'*-tetramethyldiamino)biphenyl]benzaldehyde (0.24 g, 0.90 mmol) were mixed in 50 mL of methanol. Six drops of acetic acid saturated with hydrobromic acid were added, and the mixture was refluxed for 24 h. After cooling, ~150 mL of a saturated potassium carbonate solution were added, and the solution was extracted with dichloromethane. The dichloromethane phase was dried and evaporated under vacuum. Chromatography on silica gel was accomplished by eluting with a 10:1 dichloromethane/methanol solution. The resulting compound was purified on three consecutive silica prep plates by elution with a 10:1 dichloromethane/methanol solution and yielding a small amount of pure compound (3.0 mg, 0.005 mmol, 3% yield). NMR (CD_2Cl_2) (ppm): δ –3.50 (s, 1 H, NH), –3.25 (s, 1 H, NH), 1.22 (m, 6 H, CH_2CH_3, α to the *meso*-arene), 1.85 (m, 12 H, CH_2CH_3), 2.75 ppm (s, 6 H, $N(CH_3)_2$), 2.93 (m, 4 H, CH_2CH_3, α to the *meso*-arene), 3.02 (s, 6 H, $N(CH_3)_2$, α to the biaryl bond), 3.66 (s, 6 H, CH_3), 4.05 (m, 8 H, CH_2CH_3), 6.82 (dd, J = 3.0 Hz, J' = 8.8 Hz, 1 H),), 7.02 (d, J = 3.0, 1 H, α to the biaryl bond and the $N(CH_3)_2$), 7.17 (d, J = 8.80 Hz, 1 H), 7.93 (d, J = 7.87 Hz, 2 H, α to the biaryl bond), 8.20 (d, J = 7.87 Hz, 2 H, α to the porphyrin), 9.96 (s, 1 H, meso) 10.20 (s, 1 H, meso). Calculated mass 744.4860; found 744.4 (M^+).

1-(2,7,13,18-Tetraethyl-3,8,12,17-tetramethylporphyrin-5-yl)-4-(N,N-dimethylamino)benzene (TETM-A). 1,19-Dideoxy-2,7,13,18-tetraethyl-3,8,12,17-tetramethylbiladiene-ac dihydrobromide (60 mg, 0.10 mmol) and 4-(*N,N*-dimethylamino)-benzaldehyde (0.07 g, 0.46 mmol) were mixed in 20 mL of methanol. Four drops of acetic acid saturated with hydrogen bromide were added, and the mixture was refluxed for 24 h. After cooling, 150 mL of a saturated potassium carbonate solution was added, and the mixture was extracted with dichloromethane. The dichloromethane phase was dried with sodium sulfate and evaporated under reduced pressure. Chromatography on silica gel eluting with 10:1 dichloromethane/methanol, and on alumina eluting with dichloromethane, gives an impure compound which was recrystallized from a dichloromethane/methanol solution to give 30 mg (0.050 mmol, 50% yield) of a red powder (mp >300 °C). NMR ($CDCl_3$) (ppm): δ –3.30 (br s, 2 H, NH), 1.74 (t, 6 H, CH_2CH_3), 1.87 (t, 6 H, CH_2CH_3), 2.58 (s, 6 H, $N(CH_3)_2$), 3.25 (s, 6 H, CH_3, adjacent to the *meso*-arene), 3.66 (s, 6 H, CH_3), 4.02 (m, 8 H, CH_2CH_3), 7.09 (d, J = 8.24 Hz, 2 H), 7.85 (d, J = 8.23 Hz, 2 H, C3, C5), 9.94 (s, 1 H, *meso*) 10.16 (s, 2 H, *meso*). Calculated mass 597.3851; found (FAB in nitrobenzyl alcohol matrix) 598.4 (M^+).

N-(4-(3,7,13,17-Tetraethyl-2,8,12,18-tetramethylporphyrin-5-yl)phenyl)-N'-(4'-(dimethylamino)phenyl)piperazine (TETM-AT). Bis(3-ethyl-4-methyl-2-pyrryl)(*N*-phenyl-*N'*-(4'-(dimethylamino)phenyl)piperazinyl)methane (0.79 g, 1.6 mmol) and bis(4-ethyl-5-formyl-3-methyl-2-pyrryl)methane (0.34 g, 1.2 mmol) were stirred with 100 mL of dichloromethane, 25 mL of methanol, and 5 mL of trifluoroacetic acid in a darkened vessel for 8 h. A 150-mL aliquot of a saturated potassium carbonate solution was added, and the solution was extracted with dichloromethane. The dichloromethane phase was dried with sodium sulfate and evaporated under reduced pressure. Chromatography of the residue on silica gel, eluting with dichloromethane followed by a 10:1 dichloromethane/methanol solution, yielded an impure porphyrin which was rechromatographed on alumina, eluting with a 10:1 dichloromethane/methanol solution to give 18 mg (0.024 mmol, 1.5% yield) of a pure red compound (mp >300 °C). NMR ($CDCl_3$) (ppm): δ –3.16 (s, 1 H, NH), –3.04 (s, 1 H, NH), 1.74 (t, J = 7.40 Hz, 6 H, CH_2CH_3), 1.87 (t, J = 7.65, 6 H, CH_2CH_3), 2.87 (q, J = 7.47, 8 H, CH_2CH_3), 2.96 (s, 6 H, $N(CH_3)_2$), 3.40 (m, 4 H, piperazine), 3.58 (s, 6 H, CH_3), 3.63 (m, 4 H, piperazine), 3.66 (s, 6 H, CH_3), 4.04 (q, J = 7.63 Hz, CH_2CH_3), 6.85 (d, J = 8.89 Hz, 2 H, C3' and C5'), 7.08 (d, J = 8.92 Hz, 2 H, C2', C6'), 7.25 (d, J = 7.85 Hz, 2 H, C2, C6), 8.05 (d, J = 8.42 Hz, 2 H, C3, C5), 9.93 (s, 1 H, *meso*) 10.19 (s, 2 H, *meso*). Calculated mass 757.4831; found 757.4821 (M^+).

Electrochemical Measurements. Reagent quality tetrabutylammonium perchlorate (Fluka) was recrystallized three times from ethanol and dried in a vacuum oven prior to use. *o*-Difluorobenzene (98%, Aldrich) was filtered through activated alumina, fractionally distilled, and stored over activated molecular sieves before use. Cyclic voltammograms were taken in a three chambered cell, with the counter, working, and reference electrodes arranged in a linear fashion separated by glass frits. All measurements are referenced to a saturated sodium chloride/calomel electrode with a 1-cm^2 platinum working electrode and a platinum wire counter electrode. The platinum electrodes were soaked in acid, rinsed thoroughly with water, and heated on an open flame until red hot prior to each use to remove water and ensure a fresh surface. Measurements were performed with a Princeton Applied Research programmable potentiostat. Each cyclic voltammogram was internally calibrated with the known redox couple of decamethylferrocene (–0.059 V vs SCE).

Fluorescence Measurements. Spectral-grade benzene (Fischer), butyronitrile (99+%, Aldrich), and *o*-difluorobenzene (98%, Aldrich) were deoxygenated by freeze–pump–thawing for 3–4 cycles. Solutions of the free base porphyrins in butyronitrile, benzene, and *o*-difluorobenzene were prepared under a nitrogen atmosphere and adjusted to give an absorbance of ~1 OD at the Soret maximum. Fluorescence measurements were taken on a Perkin-Elmer LS 50 fluorimeter. The quantum yields were determined by using the optically dilute method and the equation[17]

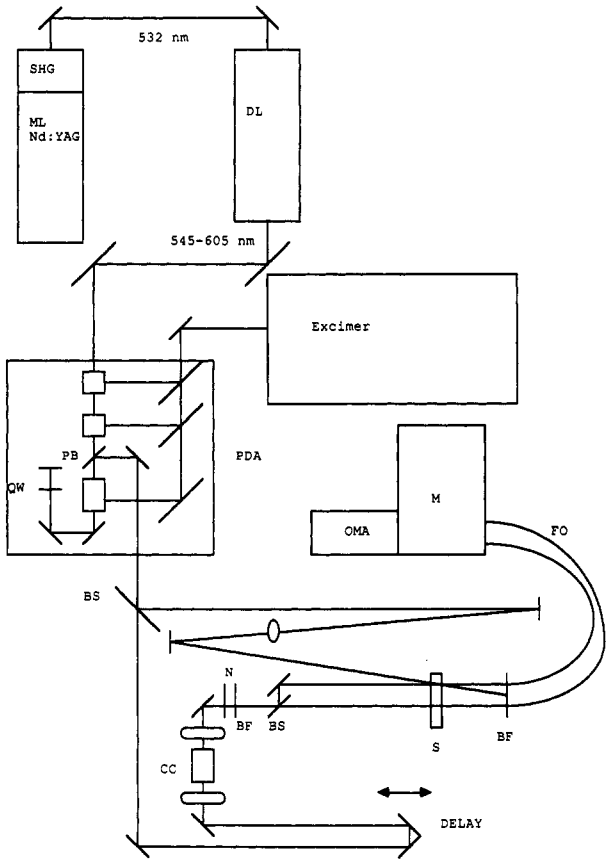

Figure 1. Schematic of the picosecond transient absorption apparatus: ML = mode locker, SHG = second harmonic generator, DL = synchronously-pumped dye laser, PDA = pulsed dye amplifier, PB = polarizing beam splitter, QW = quarter wave plate, BS = partial beam splitters, CC = continuum generation cell, N = neutral density filters, BF = band-pass filters, S = sample, FO = fiber optic cables, M = monochromator, OMA = dual diode array multichannel detector.

$$\Phi_{unk} = \Phi_{ref} \frac{A_{ref}(\lambda_{ref})}{A_{unk}(\lambda_{unk})} \frac{n_{unk}^2}{n_{ref}^2} \frac{D_{unk}}{D_{ref}}$$

where Φ is the fluorescence quantum yield, $A(\lambda)$ is the absorbance at the wavelength of excitation, n is the refractive index, D is the integrated emission intensity, and the subscripts refer to the solutions of known (ref) and unknown (unk) quantum yields. The fluorescence quantum yield standard was a solution of free base octaethyl porphyrin ($\sim$6.3 μM in the respective solvent, Φ_F = 0.13 [18]) measured concurrently. Excitation for all samples was at 530 nm.

Fluorescence lifetimes were determined by using time-correlated single photon counting at the NIH Center for Fast Kinetic Research at the University of Texas, Austin. Samples were $\sim$6 μM concentration in degassed butyronitrile. The samples were excited with 575-nm light, and the fluorescence was detected at 629 nm. The full width at half-maximum (fwhm) time response of the apparatus was 60 ± 10 ps. Fluorescent lifetimes were determined by convoluting the instrument response function with a mono- or bi-exponential decay and minimizing the χ^2 values of the fit between the predicted and experimental decays.[19]

Picosecond Absorption Spectroscopy. The picosecond transient absorption apparatus is shown in Figure 1. A Coherent 702 dye laser was synchronously pumped with the second harmonic of a Coherent Antares continuous wave (cw), mode-locked Nd:YAG laser. The dye laser was tuned to 574 nm. A background-free autocorrelation trace of the dye laser pulse is shown in Figure 2. The output of the dye laser was amplified to $\sim$200 μJ in a three-stage amplifier pumped by a Lambda-Physik EMG 102-MSC XeCl excimer laser operating at 35 Hz. At 574 nm, rhodamine

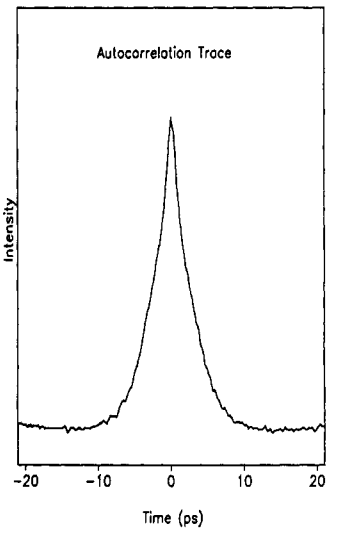

Figure 2. Background-free autocorrelation traces of the laser pulses from the synchronously-pumped dye laser with rhodamine 6G. The rhodamine 6G dye laser had a three-plate birefringent filter, and the autocorrelation trace width is 4 ± 0.5 ps.

6G was used in all three dye amplifier stages. The third stage was used in a double pass configuration, and the output beam was coupled out by using a quarter wave plate and polarizing beam splitter. ASE was spatially filtered using an Amici prism and several apertures. ASE at the sample was estimated to be ≤3% in either the pump or probe beams.

The output of the amplifier was split into two beams to generate the pump and probe by utilizing a 70%R/30%T partial beam splitter. For the probe beam, 30% of the amplified pulse was focused into a 10-cm cell containing $CHCl_3/CCl_4$ (4:6 v/v) to generate a continuum. A portion of the continuum was selected using a 380–500-nm band-pass or 575-nm long-pass filter (Oriel) and directed through an optical delay line. The probe beam was then split into two beams using a 50%T/50%R beam splitter. The pump beam was focused to a 1–1.5-mm diameter spot at the sample with a 300-mm lens. One of the probe beams and the pump beam are crossed at the sample. The other probe beam passes through an unphotoexcited part of the sample. The cross-correlation trace at the sample was measured by using the 10% and 90% points of the rise times of the ZnOEP bleach and induced absorption and was found to be 8 ± 1 ps. The transmitted probe beams are collected by a bifurcated fiber optic cable connected to a single, 0.32-m, f/4.8 monochromator (Instruments SA) coupled to a dual diode array optical multichannel detector (Princeton Instruments). Rejection of the pump beam from the spectrometer is accomplished by an identical 380–500-nm band-pass or 575-nm long-pass filter placed between the sample and collection fiber optics.

Sample solutions were prepared under a nitrogen atmosphere to a final concentration of $\sim$60 μM assuming an extinction coefficient of 159 000 cm^{-1} M^{-1} at the Soret maximum.[20] *o*-Difluorobenzene (98%, Aldrich) was deoxygenated as above and used as the solvent for all transient absorption experiments. Solutions were placed in a 1-mm path length cuvette. No evidence of irreversible photochemistry was observed in a comparison of spectra taken before and after the measurement. Experiments were repeated on at least two samples. Spectra were frequency calibrated by using Hg emission lines, and reported wavelengths are accurate to ±2 nm.

Results

Scheme I shows the *meso*-monosubstituted octaalkyl (the differing ethyl and methyl substitution patterns arose from synthetic convenience) porphyrins synthesized for this study and their abbreviations. In all of the porphyrins, the DMA and/or

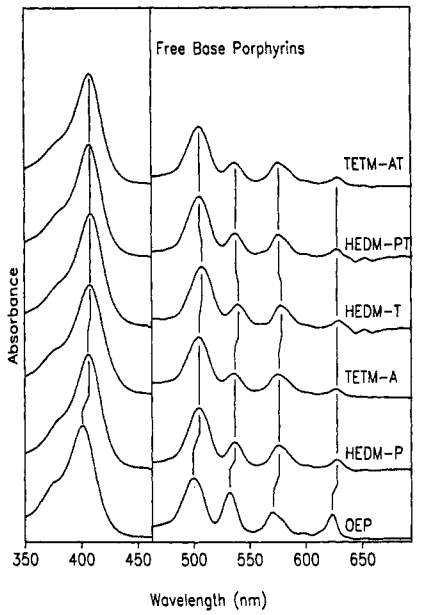

Figure 3. Ground-state absorption spectra of free base OEP and modified porphyrins in *o*-difluorobenzene. Abbreviations and structures are shown in Scheme I. The right side shows the Q-band region expanded by a factor of 6.

TMPD *meso* substituent is a potential electron donor, except for HEDM-P which served as the control. This series of porphyrins allows for comparison of charge-transfer rates from donors to porphyrins as a function of driving force and distance.

The ground-state absorption spectra for the compounds under study are shown in Figure 3. The Q and Soret bands of HEDM-P are systematically shifted 6 nm (150–350 cm^{-1}) to lower energies compared to free base octaethylporphyrins (OEP), probably as a result of electronic and/or steric effects (see Discussion). The absorption spectra of the TETM-A, HEDM-PT, and TETM-AT free base porphyrins are the same as that of free base HEDM-P, indicating no additional interaction between the donor and acceptor. However, the absorption spectrum of free base HEDM-T is red-shifted an additional 3 nm ($\sim$100 cm^{-1}) in the Q-band region. The absorption band shifts associated with HEDM-T are <100 cm^{-1} (0.01 eV) and will have little effect on the energetics of electron transfer.

The electrochemical results for the synthetic porphyrins are shown in Table I. All cyclic voltammograms exhibited good resolution and excellent signal-to-noise ratios between –2.0 and +1.2 V. All of the redox couples are reversible, single-electron events, unless otherwise noted. The reduction potentials reported for the porphyrins are close to those previously reported for free base OEP (–1.46 eV) and etioporphyrin (–1.34 eV).[21-23] The cyclic voltammogram of TETM-A exhibited an irreversible oxidation wave in all solvents, indicating that some chemistry was occurring at the electrode. The irreversible oxidation of dialkylanilines has been attributed to polymerization.[24] Pulsed radiolysis has been used to circumvent this problem and characterize the dialkylaniline cation.[25] The cyclic voltammogram of free base TETM-AT was irreversible in *o*-difluorobenzene, but reversible in THF. The porphyrin reduction, aniline oxidation, and TMPD oxidation half-wave potentials for the different porphyrins are identical within experimental error. Also, the oxidation potentials of the appended donors are consistent with the oxidation potentials of the unappended DMA (0.74 eV in CH_3CN) and TMPD (0.22 eV in CH_3CN).[26] These results indicate little to no electronic interaction between the porphyrin π-system and the electron donor.

Direct measurements of the fluorescence lifetime were obtained by using the time-correlated single photon counting technique. The results in butyronitrile are shown in Figures 4 and 5 for

TABLE I: Energetics of Free Base Donor-Appended Porphyrins[a]

porphyrin	$\Delta\epsilon_{P/P^-}$	$\Delta\epsilon_{T/T^+}$	$\Delta\epsilon_{A/A^+}$	$-\Delta U_{cs1}$[b]	$-\Delta U_{cs2}$[c]	$-\Delta U_{cr}$[d]
H_2OEP[e]	–1.46					
H_2OEP	–1.41					
H_2Etio[f]	–1.34					
H_2HEDM-P	–1.40					
H_2TETM-A[g,h]	?		?	?		?
H_2HEDM-T	–1.39	0.34		0.25		1.73
H_2HEDM-T[i]	–1.45	0.29		0.24		1.74
H_2HEDM-PT[i]	–1.43	0.31		0.24		1.74
H_2HEDM-PT	–1.42	0.34		0.22		1.76
H_2TETM-AT[g]	–1.41	0.26	0.75	–0.18	0.49	1.67

[a] All values in electronvolts. All cyclic voltammograms were measured in *o*-difluorobenzene unless otherwise indicated. The listed potentials are, from left to right, the porphyrin reduction, the TMPD oxidation, and the aniline oxidation, respectively. [b] Exothermicity of the photoinduced charge transfer from TMPD to the porphyrin in HEDM-T and HEDM-PT. Exothermicity of the photoinduced charge transfer from aniline to the porphyrin in TETM-A and TETM-AT. Calculated from $-\Delta U_{cs1} = E_{S1} - E_D^{ox} + E_P^{red}$ where E_{S1} = 1.98 eV and E_D^{ox} and E_P^{red} are the donor oxidation and porphyrin reduction potentials, respectively. [c] Exothermicity of the photoinduced charge transfer from TMPD to the aniline cation for TETM-AT. Calculated from $-\Delta U_{cs2} = E_T^{ox} - E_{An}^{red}$ where E_{S1} = 1.98 eV and E_T^{ox} and E_{An}^{red} are the TMPD oxidation and aniline cation reduction potentials, respectively. [d] Exothermicity of the charge recombination between the porphyrin anion and donor cation. Calculated from $-\Delta U_{cs2} = E_d^{red} - E_P^{ox}$ where E_{S1} = 1.98 eV and E_P^{ox} and E_D^{red} are the porphyrin anion oxidation and donor cation reduction potentials, respectively. [e] From ref 22. [f] From refs 23 and 21. [g] In THF. [h] Irreversible. [i] In butyronitrile.

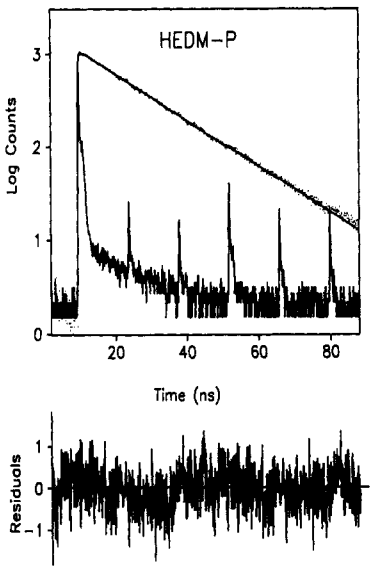

Figure 4. Time-correlated single photon counting measurements of the fluorescence lifetime of HEDM-P. The data were analyzed by deconvoluting the instrument response function (top, noisy spectrum) with a single-exponential decay (top, solid line) such that the residuals (bottom) are minimized. For HEDM-P this analysis yields a lifetime of 17 ns with a reduced χ^2 of 1.10.

HEDM-P and HEDM-PT, respectively. For HEDM-P, the fluorescence decay was fit to a single exponential with a characteristic lifetime of 17 ns and a reduced χ^2 value of 1.10. For HEDM-PT, two components with characteristic lifetimes of 2 ns (95% amplitude) and 16 ns (5% amplitude) were necessary to accurately fit the fluorescence decay with a reduced χ^2 of 0.94. The lifetime measurements of 17 ns for HEDM-P and 2 ns for HEDM-PT are in good agreement with fluorescence quenching studies (Table II) of HEDM-P and HEDM-PT in butyronitrile within the experimental error of ±30% for the quenching studies. The small, 16-ns component in HEDM-PT is probably due to molecules in which the TMPD has been air-oxidized. As a result, charge transfer is blocked and the fluorescence decay is identical to the HEDM-P control. No attempt was made to temporally

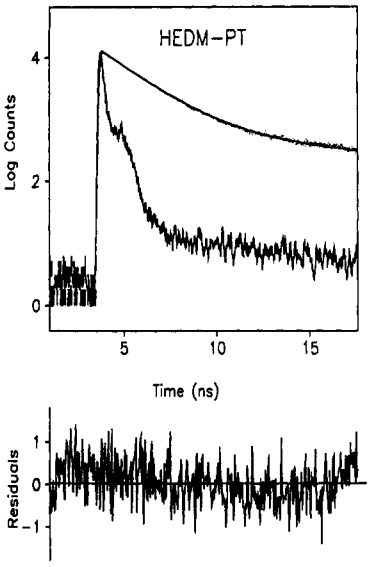

Figure 5. Time-correlated single photon counting measurements of the fluorescence lifetime of HEDM-PT. The data were analyzed as in Figure 4 with a two component fit to yield lifetimes of 2 ns (95%) and 16 ns (5%) with a reduced χ^2 of 0.95. The small, slower component is probably due to HEDM-PT in which the TMPD has been oxidized.

TABLE II: Fluorescence Quantum Yields and Singlet-State Lifetimes of Free Base Donor-Appended Porphyrins in Various Solvents

porphyrin	solvent	ΔG_{solv}[a]	relative ϕ_F[b]	τ_s[c]
H_2HEDM-P	benzene		0.59	11.2 ns
H_2TETM-A	benzene	–0.92, –0.70	0.43	8.1 ns
H_2HEDM-T	benzene	–0.92, –0.70	0.0005	9.5 ps
H_2HEDM-PT	benzene	–0.52, –1.05	0.65	12.3 ns
H_2TETM-AT	benzene	(–0.92, –0.60), (–0.70, –0.65)	0.44	8.3 ns
H_2HEDM-P	butyronitrile		0.56	10.6 ns
H_2TETM-A	butyronitrile	–0.092	0.66	12.5 ns
H_2HEDM-T	butyronitrile	–0.092	0.0005	9.5 ps
H_2HEDM-PT	butyronitrile	–0.052	0.080	1.5 ns
H_2TETM-AT	butyronitrile	–0.092, –0.060	0.50	9.5 ns
H_2HEDM-P	*o*-difluorobenzene		0.32	6.0 ns
H_2TETM-A	*o*-difluorobenzene	–0.17	0.56	10.6 ns
H_2HEDM-T	*o*-difluorobenzene	–0.17	0.00008	1.5 ps
H_2HEDM-PT	*o*-difluorobenzene	–0.095	0.067	1.3 ns
H_2TETM-AT	*o*-difluorobenzene	–0.17, –0.11	0.51	9.6 ns

[a] Solvation free energy for the charge separated state. Values are in electronvolts. For the ΔG_{solv} values in benzene, the first number is the Coulomb free energy calculated from $\Delta G_{solv} = e_0/4\pi\epsilon_0\epsilon a$, where a is the center-to-center separation and ϵ is the static dielectric constant. The second value is the ΔG_{solv} calculated from refs 45 and 46 using *o*-difluorobenzene as the reference solvent. For TETM-AT in benzene, the first set of numbers is the values applicable to the A → P charge-transfer step and the second set of numbers is the values applicable to the T → A charge transfer. The values in butyronitrile and *o*-difluorobenzene are the Coulomb term only. [b] Fluorescence quantum yield, measured relative to H_2OEP in each solvent. [c] Excited singlet-state lifetime of the competing process, τ_S, was calculated from $\tau_S = \tau_S\phi/\phi_0$, where τ_S and ϕ_0 are the singlet lifetime (18.9 ns) and fluorescence quantum yield (0.13) of H_2OEP[18] and ϕ is the fluorescence quantum yield of the modified porphyrin.

resolve the fluorescence lifetime of HEDM-T since the fluorescence quenching studies had shown the lifetime to be ≤9 ps in all solvents (see below), well beyond the time resolution of the system.

Table II shows the relative fluorescence quantum yields and excited singlet-state lifetimes of these synthetic porphyrins in a variety of solvents. The excited-state lifetimes were calculated directly from the relative fluorescence quantum yields, measured with respect to H_2OEP, and have an estimated experimental error of ±30%. The shapes of the fluorescence emission spectra were not perturbed from those of free base OEP by the presence of an additional *meso*-substitution. HEDM-P showed some quenching of fluorescence compared to free base OEP in all solvents. This has been shown to occur in *meso*-tetrasubstituted octaalkylporphyrins[27] and may arise from increased intersystem crossing and/or internal conversion from the lowest excited singlet state. The fluorescence quenching of HEDM-P is consistent with an excited state singlet lifetime of 11 ± 4 ns. Substantial fluorescence quenching of HEDM-T and HEDM-PT is observed in the polar solvents. In benzene solution, fluorescence from HEDM-T is quenched, but no quenching is observed for HEDM-PT. Benzene should have a higher solvent reorganizational energy for charge transfer in HEDM-PT than HEDM-T because of the greater distance between charged species in the former. Thus, the charge-transfer rate becomes slower than the fluorescence rate for HEDM-PT, but it remains fast enough in HEDM-T to compete with fluorescence. The lifetimes reported for HEDM-T should be taken as upper limits. The fluorescence is so weak from HEDM-T that it was difficult to obtain an accurate measurement of the fluorescence quantum yield. The lack of a strong solvent effect on the kinetics of charge separation was also observed in a quinone–porphyrin in which the quinone is directly attached to the porphyrin.[28] Because the fluorescence quenching in HEDM-T and HEDM-PT is strong, the quenching due to the phenyl group plays only a minor role in the determination of the excited-state relaxation time. Thus, the charge-transfer rate constant can be calculated directly from $1/\tau_s$. These data indicate that intramolecular charge transfer is the most important excited-state deactivation process in the TMPD donor-appended octaalkylporphyrins.

The aniline derivatives, TETM-A and TETM-AT, fail to show significant fluorescence quenching in any solvent, indicating that aniline is an ineffective donor. The driving force for charge transfer to the porphyrin singlet state is in fact uphill (see below). In the case of TETM-AT, charge transfer might have been expected from the TMPD group, by analogy with HEDM-PT, but, as discussed below, the spacer in TETM-AT is long enough to preclude charge transfer during the excited-state lifetime. The lack of observed fluorescence quenching in these derivatives, in which the charge-transfer state lies above the lowest-lying singlet excited state, implies that charge transfer is the dominant deactivation pathway in the TMPD-appended porphyrins.

The definitive test of charge separation, however, is direct observation of the charge separated species. Previous studies have indicated that characterization of porphyrin excited-state species is difficult at wavelengths <500 nm due to overlapping absorption bands of the singlet, triplet, and radical species.[29] To observe the charge separated species, picosecond transient absorption measurements were carried out at wavelengths from 590 to 660 nm for free base HEDM-T and HEDM-PT. The absorption bands of $TMPD^+$ lie at ~565 and ~606 nm with extinction coefficients of ~12 000 cm^{-1} M^{-1} and fwhm band widths of ~20–75 nm.[30] Although the TMPD+ absorption band at 565 nm is buried in the bleach of the Q-band at 572 nm and the scattering from the intense pump beam at 574 nm, the induced absorption band at 606 nm should be observable. The results are shown in Figure 6A,B. In these spectra, the bleach of the Q-band at 628 nm and an induced absorption which we assign to the TMPD+ species at 606 nm are clearly seen. Scattered light from the pump beam and the bleach due to the 574-nm Q-band can be seen at wavelengths <580 nm. The smaller induced absorption of HEDM-PT vs HEDM-T is a result of the smaller rate constant for charge separation in HEDM-PT. The observation of the donor cation absorption is conclusive evidence that charge transfer is the dominant excited-state deactivation pathway in these TMPD-appended porphyrins.

To measure the rates of charge recombination in the TMPD-appended porphyrins, picosecond transient absorption spectroscopy was carried out at wavelengths between 360 and 460 nm.

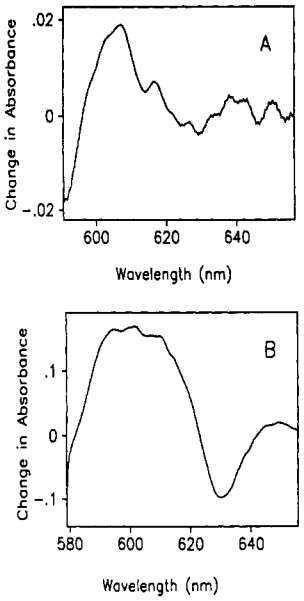

Figure 6. (A) Transient absorption spectra in the Q-band region of free base HEDM-T. Excitation was at 574 nm with a ~4-ps pulse. The time delay was 15 ps. (B) Transient absorption spectra in the Q-band region of free base HEDM-PT. Excitation was at 574 nm with a ~4-ps pulse. The time delay was 1.0 ns. In both spectra, the induced absorption at 606 nm is assigned as the $TMPD^+$ absorption.

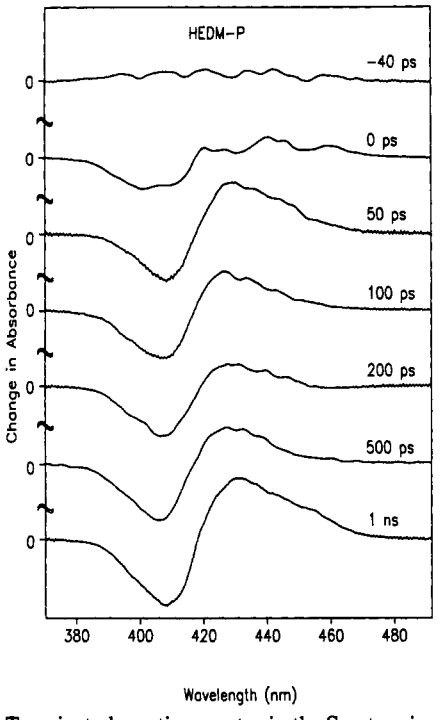

Figure 7. Transient absorption spectra in the Soret region of free base HEDM-P. Excitation was at 574 nm with a ~4-ps pulse. A slight evolution in the induced absorption and the Soret bleach is evident at times >200 ps and indicates formation of the triplet state. The Soret bleach is 0.05 OD at 100 ps.

The results are shown in Figures 7–9. All spectra show a bleach of the ground-state Soret absorption. The transient spectra of the HEDM-P reference molecule (Figure 7) show an induced absorption from ~420 to 460 nm that peaks at 431 nm, consistent with the previously reported transient spectrum of the $S_1 \rightarrow S_n$ absorption in free base OEP.[31] A slight evolution of the spectrum is seen at 500 ps and 1 ns. The Soret bleach gets slightly deeper, and the induced absorption shifts slightly to the red. This is consistent with formation of the triplet, which peaks at ~438 nm.[31] With an 11-ns S_1 lifetime and with the assumption of an ISC $S_1 \rightarrow T_1$ quantum yield of 0.9 as seen in other free base

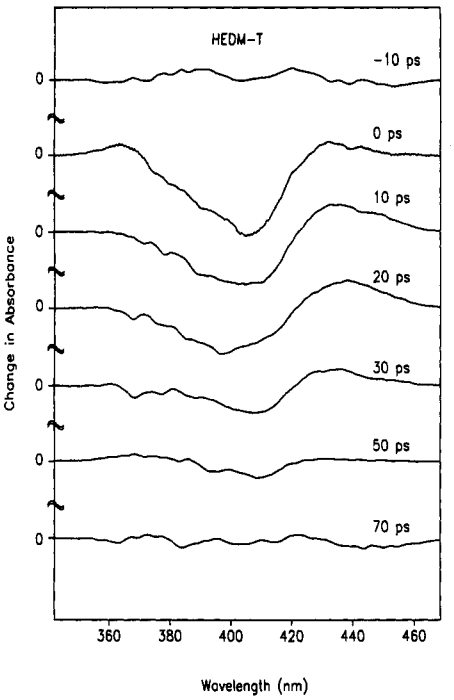

Figure 8. Transient absorption spectra in the Soret region of free base HEDM-T. Excitation was at 574 nm with a ~4-ps pulse. The Soret bleach recovery and induced absorption decay are essentially complete by 50 ps. The Soret bleach is 0.03 OD at 10 ps.

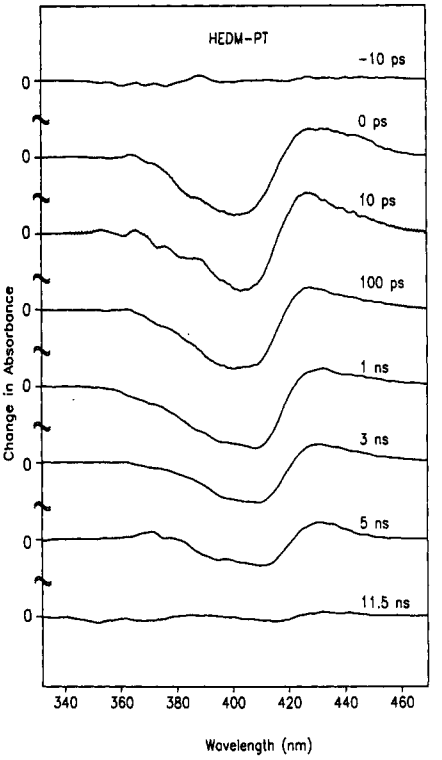

Figure 9. Transient absorption spectra in the Soret region of free base HEDM-PT. Excitation was at 574 nm with a ~4-ps pulse. The Soret bleach recovery and induced absorption decay are complete by 11.5 ns. The Soret bleach is 0.05 OD at 100 ps.

porphyrins,[32] approximately 10% of the population in the singlet will have crossed to the triplet state in 1 ns.

The transient absorption spectra of HEDM-T show a broad Soret bleach at ~400 nm and a broad induced absorption from 420 to 460 nm that peaks at ~430 nm (Figure 8). Although no absorption spectra of free base octaalkyl porphyrin anion radicals have been reported, the anion radicals of metallooctaalkylporphyrins all show absorption bands ~1800 cm^{-1} (30 nm) to lower

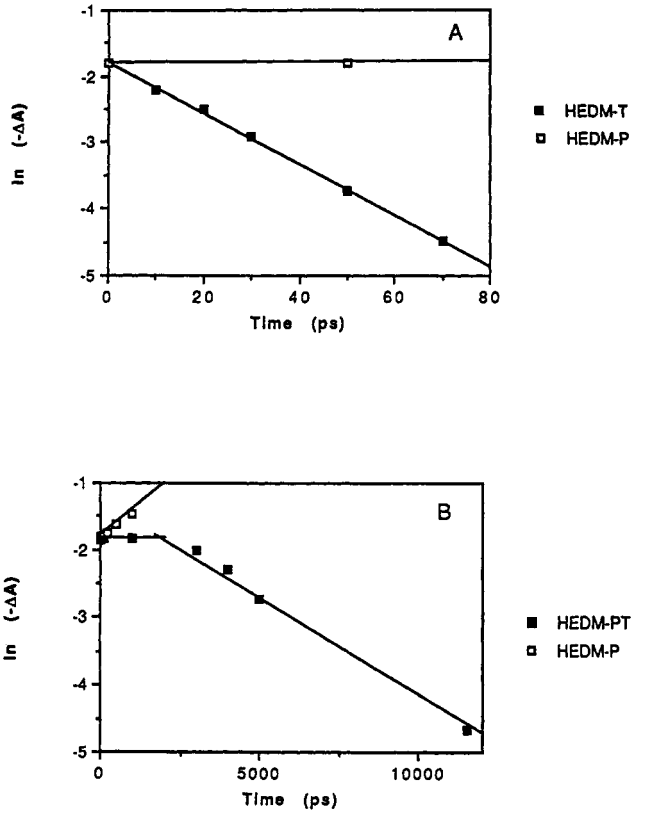

Figure 10. Soret bleach recovery kinetic plots of (A) HEDM-T and (B) HEDM-PT free base porphyrins in *o*-difluorobenzene. The ΔA values were taken at 402 nm in both A and B. The lines are the least-squares fits to the points and yielded regression coefficients of 0.99 for HEDM-T and 0.97 for HEDM-PT. The increase in bleach for the HEDM-P non-charge-transfer complex in B is a result of formation of the triplet state (see text).

energies from the ground-state Soret absorption.[33] Since the fluorescence quenching studies indicate $S_1 \rightarrow$ CT state crossing in 1.5 ps in *o*-difluorobenzene, we ascribe the induced absorption to the $HEDM^-T^+$ CT state. The Soret bleach recovery and decay of the induced absorption for HEDM-T is complete within 50 ps. First-order kinetic analysis was performed on the recovery of the Soret bleach to quantitatively determine the charge recombination rate (Figure 10A). The Soret region was used for two reasons. First, the high signal-to-noise ratio in this region of the spectrum allows for a more precise determination of the recovery kinetics. Second, the fact that all of the excited states have some absorption in this spectral region enables the determination of the kinetics of state crossings. For HEDM-T, the charge recombination rate is $(3.8 \pm 0.4) \times 10^{10}$ s^{-1} with a linear regression coefficient of $r = 0.99$, yielding a lifetime for the charge-transfer state of 26 ± 3 ps.

The transient absorption spectra of HEDM-PT show a broad Soret bleach at ~404 nm and a broad induced absorption from 420 to 475 nm (Figure 9). The Soret bleach recovery and decay of the induced absorption are complete within 7–10 ns with no evidence of a long-lived triplet state. Free base porphyrins typically exhibit a high quantum yield (ca. 0.8) for triplet formation.[32] The 1.3-ns rise time of the charge-transfer state from fluorescence quenching studies and the lack of any long-lived transients attributable to a triplet state imply that the excited-state of HEDM-PT deactivates primarily through a $HEDM^-PT^+$ charge-transfer state. First-order kinetic analysis of the Soret bleach recovery of HEDM-PT gives a charge recombination rate of $(2.9 \pm 0.3) \times 10^8$ s^{-1} with a linear regression coefficient of $r = 0.97$, yielding a charge-transfer-state lifetime of 3.5 ± 0.4 ns (Figure 10B). The lack of spectral evolution of the transient spectra is to be expected since the porphyrin excited-state and anion radical absorption spectra in this region are similar and no significant amount of triplet state is formed (see above). The pause in the early time course of the decay of HEDM-PT (Figure 10B) reflects the conversion from the excited singlet state to the CT state. Then, as the CT state decays, the ground-state recovery is seen as the decrease in $\ln(-\Delta A)$ with increasing time. The slow increase in the measured induced absorption of the HEDM-P (Figure 10B) reflects conversion of the singlet to the triplet excited state, which has a higher transmittance at the monitoring wavelength (404 nm).

Discussion

The red shifts observed in the absorption spectra of the *meso*-substituted porphyrins can be attributed to electronic and steric effects on the HOMO's of an octaalkylporphyrin. Red shifts of the Soret and Q-bands on going from H_2OEP to H_2TPP are ascribed to an electronic effect. In the four-orbital model of porphyrin electronic states,[34] the HOMO's are the a_{1u} and a_{2u} molecular orbitals. The phenyl groups destabilize the a_{2u} orbital, which has large coefficients at the *meso* carbon atoms, leading to a ~500–1100-cm^{-1} red shift in all of the absorption bands because of the resulting decrease in the HOMO–LUMO gap. A larger red shift, ~2400 cm^{-1}, is seen when phenyl groups are substituted at the four *meso* positions of H_2OEP. In the resulting H_2OETPP, the porphyrin ring is severely ruffled due to the steric clash between the ethyl and phenyl substituents.[27] INDO/s calculations and measurements of the redox potentials of H_2OETPP show that the HOMO's are destabilized and the LUMO is unaffected by the puckering of the porphyrin macrocycle.[27,35] The phenyl-appended porphyrin reported here shows a smaller red shift than H_2OETPP or H_2TPP, reflecting the smaller perturbation associated with a single phenyl substituent. The greater red shift of HEDM-T than any other of the porphyrins is indicative of a slight interaction between the TMPD amino groups and the porphyrin π-electronic structure. Slight red shifts in the Q-band region have been seen in free base TPP's with amines ortho to the porphyrin linkage.[36] Electron-donating groups in this position will slightly raise the a_{2u} orbital energy by donating extra electron density to the porphyrin carbons and may also slightly raise the a_{1u} orbital by interactions with the adjacent pyrrole carbons. The Q_{y0} and Q_{x0}-bands are also more intense in free base OEP than in the *meso*-monosubstituted porphyrins (Figure 3). Because the a_{1u} is the higher energy HOMO, a destabilization of the a_{2u} MO decreases the a_{1u}–a_{2u} gap. As the a_{1u}–a_{2u} gap decreases, configuration interaction increases, leading to decreased Q_{x0} and Q_{y0} absorption intensities and increased B absorption intensity.[37,38]

The steric effect on the electronic structure of *meso*-substituted octaalkylporphyrins can also be observed in the fluorescence quantum yields. A previous study of H_2OETPP demonstrated a lower fluorescence quantum yield compared to the octaethylporphyrin free base.[27] This effect is likewise attributable to the saddle distortion induced in the porphyrin macrocycle by the steric crowding of the ethyl and phenyl substituents.[27] The out-of-plane distortion may increase internal conversion and/or intersystem crossing. HEDM-P also shows modest fluorescence quenching compared to free base OEP.

Much greater fluorescence quenching is seen for free base HEDM-T and HEDM-PT, indicating a charge-transfer mechanism for excited-state deactivation. HEDM-PT shows fluorescence quenching only in butyronitrile and *o*-difluorobenzene, while HEDM-T shows fluorescence quenching in all solvents (Table II). The lack of fluorescence quenching for HEDM-PT in benzene is attributed to the higher solvent reorganizational energy. The greater solvent reorganizational energy in benzene decreases the driving force and, consequently, the rate of the reaction. Thus, the charge separation can no longer compete with the singlet-state lifetime, and no fluorescence quenching is

seen. Free base etioporphyrin has a singlet lifetime of 19 ns and efficiently ($\Phi_{ISC} \sim 0.8$) intersystem crosses to the lowest triplet.[32] The fluorescence lifetimes of HEDM-T and HEDM-PT are reduced to 1.5 ps and 1.3 ns, respectively, in *o*-difluorobenzene. The transient absorption measurements show charge recombination occurring with 26-ps and 3.5-ns lifetimes for HEDM-T and HEDM-PT, respectively. In the transient absorption experiments, we see no evidence of long-lived triplet formation in either of the TMPD-appended porphyrins. Using the rate constants for ISC and charge separation, we estimate the amount of triplet state formed in either porphyrin to be less than the smallest detectable difference for the apparatus.

By using the difference absorption spectrum and the extinction coefficients of the 628-nm porphyrin Q-band ($\epsilon = 5000 \pm 500$ cm^{-1} M^{-1}) and of the 606-nm $TMPD^+$ band ($\epsilon = 11\,500$ cm^{-1} M^{-1}), a measure of the charge separation efficiency can be obtained. With use of these values for the extinction coefficients and absorbances of 0.019 OD for the $TMPD^+$ and 0.0097 OD for the porphyrin bleach, the charge separation yield is 70 ± 17%. This value is consistent with the lack of observation of the triplet state in the HEDM-T picosecond transient absorption spectra. With use of the same values for the HEDM-PT extinction coefficients and absorbances of 0.17 OD for the $TMPD^+$ and 0.12 OD for the porphyrin bleach, the charge separation yield is 50%. The remaining excited-state population must decay by fluorescence to the singlet ground state.

It is instructive to consider the factors affecting the rate of charge separation in these systems and compare the experimental charge separation rates to the calculated rates from the Marcus theory of electron transfer. The charge separation rate is given by[39]

$$k_{cs} = \frac{2\pi}{h} H_{ab}^{\,2} \exp\left\{-\frac{(\Delta G^\circ + \lambda)^2}{4\lambda RT}\right\} \qquad (1)$$

where H_{ab} is the matrix element describing the coupling between the electronic states of the reactants and products, λ is the reorganizational energy, and ΔG° is the standard free energy of charge separation.

In the adiabatic regime, the electronic coupling is strong. For adiabatic charge transfers, the pre-exponential factor is usually replaced by v_0 and the rate is determined from classical transition-state theory. In the non-adiabatic case, the electronic coupling is smaller and the electronic coupling matrix element can be written as $H_{ab}^2 = H_{ab,0}^2 \exp\{-\beta(r - r_0)\}$, where $H_{ab,0}$ is the purely electronic coupling matrix element, β is an empirical constant describing the distance dependence of electron transfer, r is the shortest center-to-center reactant nuclear distance, and r_0 is roughly the van der Waals radii of donor and acceptor.[39] For the systems presented here, no evidence of electronic communication between the donor and acceptor is observed in either the absorption spectra or the cyclic voltammograms. We believe that the charge transfer in all systems but HEDM-T is occurring in the non-adiabatic regime. For HEDM-T, it is unclear whether the charge transfer is adiabatic or non-adiabatic. The rate and the slight interaction between donor and porphyrin observed in the absorption spectrum suggest that the electronic coupling is higher for HEDM-T than the other modified porphyrins. Stronger electronic coupling might be expected because of the availability of a pathway for through-space charge transfer in HEDM-T due to the positioning of the TMPD amino group over the porphyrin ring (Scheme I). However, the lack of any observable charge-transfer absorption or emission precludes the quantitative determination of the electronic coupling matrix element.

Some measure of the distance dependence in TMPD-appended free base porphyrins can be determined from a comparison of the rates of charge separation and recombination of the TMPD-appended and phenyl–TMPD-appended free base porphyrins. Assuming the electronic coupling and the reorganizational energy are the same for the two porphyrins in the same solvent, the distance dependence can be found from the ratio of the rate constants $k_{cs1}/k_{cs2} = \exp\{-\beta(r_1 - r_2)\}$, where k_{cs1} and r_1 are for the TMPD-appended porphyrin and k_{cs2} and r_2 are for the phenyl–TMPD-appended porphyrin. With use of $r_1 - r_2 = 6$ Å for the phenyl spacer diameter, a β of 1.1 $Å^{-1}$ is obtained from the ratio of the fluorescence quenching rate constants in *o*-difluorobenzene. In butyronitrile, the ratio of the charge separation rate constants yields $\beta = 0.87$ $Å^{-1}$. By using the charge recombination rate constants as measured in *o*-difluorobenzene, $\beta = 0.82$ $Å^{-1}$ is obtained. These values of β are similar, but slightly lower than those observed in quinones appended to octamethyl free base porphyrins through 1,4-disubstituted bicyclo(2.2.2)octane spacers.[10,40] The presence of the unsaturated phenyl spacer in the phenyl–TMPD-appended porphyrin opens up the possibility of superexchange, in which the low-energy π-orbitals of the phenyl spacer group may be directly involved in the charge transfer.[41] The participation of the phenyl π-orbitals in the charge transfer should lead to a smaller distance dependence to the rate of charge transfer and, consequently, a smaller value of β. However, the values of β obtained are fairly consistent with the values obtained in systems with saturated spacer groups and suggest minimal π-orbital superexchange[4] is occurring, probably because the ≥62° angle between the porphyrin and benzene ring planes[42] severely limits the amount of molecular orbital overlap. NMR studies of tetraphenylporphyrins have shown no electronic communication between the phenyl group and the porphyrin ring in the ground state.[43,44]

As pointed out above, both TETM-A and TETM-AT fail to show any fluorescence quenching. Therefore, no charge transfer is occurring in these systems within the excited-state lifetime. In the case of TETM-A, the energetics of charge transfer between aniline and porphyrin is probably unfavorable. Although the cyclic voltammogram of TETM-A exhibited irreversibility, the potentials observed for TETM-AT can be used to approximate the energetics of charge transfer. From Table I, it can be seen that the exothermicity ($-\Delta G_{cs}$) for the photoinduced charge transfer from aniline to porphyrin is −180 mV. Because the exothermicity is negative, the charge transfer is energetically unfavorable. Likewise, the charge transfer between the aniline and porphyrin in TETM-AT is energetically unfavorable (Table I). It might have been expected that the TMPD donor would quench the porphyrin excited state in TETM-AT, as it does in HEDM-T and HEDM-PT. The spacer, however, is longer in TETM-AT than in HEDM-PT (see Scheme III) by an estimated 5–6 Å. If $\beta = 1.1$ $Å^{-1}$ for both compounds, then the charge separation rate constant is expected to decrease by 3 or 4 orders of magnitude in TETM-AT, to a value of $\sim 7.7 \times 10^4$ s^{-1}. This would be too slow to effectively compete with intersystem crossing to the triplet state, $k_{ISC} = 4.2 \times 10^7$ s^{-1}.

The exothermicity ($-\Delta G$) of the photoinduced electron transfer and charge recombination is[8]

$$-\Delta G_{cs} = E_{S1} - E_D^{ox} + E_A^{red} + \Delta G_{solv} \qquad (2)$$

$$-\Delta G_{cr} = E_D^{ox} - E_A^{red} - \Delta G_{solv} \qquad (3)$$

where E_{s1} is the energy of the lowest-lying excited state, E_D^{ox} and E_A^{red} are the measured $E_{1/2}$ potentials for the one-electron oxidation of TMPD and reduction of porphyrin, respectively, and ΔG_{solv} is the solvent free energy change. If the electrochemical redox potentials, singlet energies, and charge-transfer kinetics are all measured in the same solvent, then $\Delta G_{solv} = -e_0/4\pi\epsilon_0\epsilon a$ is simply the Coulomb stabilization energy due to charge separation, where ϵ is the static dielectric constant and a is the center-to-center separation.

If the redox potentials and kinetics are measured in different solvents, the Born equation can be applied to a treatment of the

energetics of solvation.[45,46] Several of the charge-transfer studies on porphyrin-linked quinones have used this correction to calculate free energies.[6,8,47] We have explored the applicability of this correction to the donor-appended porphyrins by comparing the measured and calculated free energy of solvation of HEDM-T and HEDM-PT in butyronitrile and *o*-difluorobenzene. From Table I it can be seen that the photoelectrochemical driving force ΔU for charge separation changes 10–20 mV between *o*-difluorobenzene and butyronitrile. However, we calculated the correction from this equation to be 90 mV, much larger than the 10–20 mV observed experimentally. The discrepancy probably arises from the neglect of differences in the optical dielectric response, ϵ_{op}. Schmidt et al. have recently shown that this correction predicts the wrong free energy dependence to the charge-transfer rate constant, by examining the rate of charge transfer in a porphyrin–benzamide–quinone charge-transfer complex in solvents with dielectric constants ranging from 4 to 36.[48]

The electron-transfer rates observed in these porphyrin–donors are similar to those in porphyrin–acceptor complexes. A ≤350-fs charge separation time has been measured in an octaalkylporphyrin directly linked to a quinone.[49] In complexes in which the octaalkylporphyrin and benzoquinone were separated by a phenyl spacer, the charge separation time was ~400 ps.[10] Thus, charge separation for quinones is ~4 times faster than for TMPD, when both are separated from the porphyrin by a phenyl spacer. The increased rate is attributable to the enhanced exothermicity for charge transfer to quinone, ~0.5 eV[9], relative to that for charge transfer from TMPD, ~0.2 eV. The ~0.3-eV difference is expected to produce roughly an 8× increase in the rate, according to previous studies on the free energy dependence of the rate of charge separation in porphyrin–quinone complexes.[8] It can be concluded that the electron-transfer process does not differ qualitatively for porphyrins acting as donors or acceptors.

Acknowledgment. The authors thank Phillip Reid and Stephen Doig for useful discussions and John Eng for technical help with the transient absorption spectroscopy. The fluorescence lifetime measurements were made with the generous assistance of the NIH Center for Fast Kinetic Research, which is supported by the Division of Research Resources of the NIH and by the University of Texas at Austin. This work was supported by DOE Grant DE-FG02-88ER13876 to T.G.S. and NIH Grants GM35208 and GM31946 to A.D.H. G.R.L. is supported by NIH NRSA Fellowship GM13611. Equipment support was provided by the State of New Jersey through the Princeton Center for Photonics and Opto-Electronic Materials.

References and Notes

(1) Hoffman, B. M.; Natan, M. J.; Nocek, J. M.; Wallin, S. A. *Struct. Bonding (Berlin)* **1991**, *75* (Long-range Electron Transfer in Biology), 85–108.

(2) Gunner, M. R. In *Current Topics in Bioenergetics*; Lee, C. P., Ed.; Academic: New York, 1991; pp 319–367.

(3) Debus, R. J.; Barry, B. A.; Sithole, I.; Babcock, G. T.; McIntosh, L. *Biochemistry* **1988**, *27*, 9071–9074.

(4) Wasielewski, M. R. *Chem. Rev.* **1992**, *92*, 435–461.

(5) Gust, D.; Moore, T. A.; Moore, A. L.; Makings, L. R.; Seely, G. R.; Ma, X.; Trier, T. T.; Gao, F. *J. Am. Chem. Soc.* **1988**, *110*, 7567–7569.

(6) Gaines, G. L., III; O'Neil, M. P.; Svec, W. A.; Niemczyk, M. P.; Wasielewski, M. R. *J. Am. Chem. Soc.* **1991**, *113*, 719–721.

(7) Wasielewski, M. R.; Johnson, D. G.; Svec, W. A.; Kersey, K. M.; Cragg, D. E.; Minsek, D. W. In *Photochemical energy Conversion*; Norris, J. R., Meisel, D., Eds.; Elsevier: New York, 1989; pp 135–147.

(8) Wasielewski, M. R.; Niemczyk, M. P.; Svec, W. A.; Pewitt, E. B. *J. Am. Chem. Soc.* **1985**, *107*, 1080–1082.

(9) Wasielewski, M. R.; Niemczyk, M. P. *J. Am. Chem. Soc.* **1984**, *106*, 5043–5045.

(10) Joran, A. D.; Leland, B. A.; Geller, G. G.; Hopfield, J. J.; Dervan, P. B. *J. Am. Chem. Soc.* **1984**, *106*, 6090–6092.

(11) Harriman, A.; Kubo, Y.; Sessler, J. L. *J. Am. Chem. Soc.* **1992**, *114*, 388–390.

(12) Sessler, J. L.; Johnson, M. R.; Lin, T.-Y.; Creager, S. E. *J. Am. Chem. Soc.* **1988**, *110*, 3659–3661.

(13) Sakata, Y.; Nakashima, S.; Goto, Y.; Tatemitsu, H.; Misumi, S.; Asahi, T.; Hagihara, M.; Nishikawa, S.; Okada, T.; Mataga, N. *J. Am. Chem. Soc.* **1989**, *111*, 8979–8981.

(14) Liu, J.-Y.; Schmidt, J. A.; Bolton, J. R. *J. Phys. Chem.* **1991**, *95*, 6924–6927.

(15) Harriman, A.; Hosie, R. J. *J. Photochem.* **1981**, *15*, 163–167.

(16) Wasielewski, M. R.; Gaines, G. L., III; O'Neil, M. P.; Svec, W. A.; Niemczyk, M. P. *J. Am. Chem. Soc.* **1990**, *112*, 4559–4560.

(17) Demas, J. N.; Crosby, G. A. *J. Phys. Chem.* **1971**, *75*, 991–1024.

(18) Ohno, O.; Kaizu, Y.; Kobayashi, H. *J. Chem. Phys.* **1985**, *82*, 1779–1787.

(19) O'Connor, D. V.; Phillips, D. *Time Resolved Single Photon Counting*; Academic Press: London, 1984.

(20) Smith, K. M. *Porphyrins and Metalloporphyrins*; Elsevier: New York, 1975.

(21) Clack, D. W.; Hush, N. S. *J. Am. Chem. Soc.* **1965**, *87*, 4238–4242.

(22) Fuhrhop, J.-H.; Kadish, K. M.; Davis, D. G. *J. Am. Chem. Soc.* **1973**, *95*, 5140–5147.

(23) Felton, R. H.; Linschitz, H. *J. Am. Chem. Soc.* **1966**, *88*, 1113–1116.

(24) Bettelheim, A.; White, B. A.; Raybuck, S. A.; Murray, R. W. *Inorg. Chem.* **1987**, *26*, 1009–1017.

(25) Kadish, K. M.; Cornillon, J.-L.; Yao, C.-L.; Malinski, T.; Gritzner, G. *J. Electroanal. Chem.* **1987**, *235*, 189–207.

(26) Reed, R. C.; Wightman, R. M. In *Encyclopedia of Electrochemistry of the Elements*; Bard, A. J., Lund, H., Eds.; Dekker: New York, 1984; pp 1–165.

(27) Barkigia, K. M.; Berber, M. D.; Fajer, J.; Medforth, C. J.; Renner, M. W.; Smith, K. M. *J. Am. Chem. Soc.* **1990**, *112*, 8851–8857.

(28) Bergkamp, M. A.; Dalton, J.; Netzel, T. L. *J. Am. Chem. Soc.* **1982**, *104*, 253–259.

(29) Holten, D. H.; Gouterman, M. In *Optical Properties and Structure of Tetrapyrroles*; Blauer, G., Sund, H., Eds.; de Gruyter: New York, 1985; pp 63–90.

(30) Albrecht, A. C.; Simpson, W. T. *J. Am. Chem. Soc.* **1955**, *77*, 4454–4461.

(31) Rodriguez, J.; Kirmaier, C.; Holten, D. *J. Am. Chem. Soc.* **1989**, *111*, 6500–6506.

(32) Darwent, J. R.; Douglas, P.; Harriman, A.; Porter, G.; Richoux, M.-C. *Coord. Chem. Rev.* **1982**, *44*, 83–126.

(33) Stolzenberg, A. M.; Stershic, M. T. *J. Am. Chem. Soc.* **1988**, *110*, 6391–6402.

(34) Gouterman, M. In *The Porphyrins*; Dolphin, D., Ed.; Academic Press: New York, 1978; pp 1–165.

(35) Barkigia, K. M.; Chantranupong, L.; Smith, K. M.; Fajer, J. *J. Am. Chem. Soc.* **1988**, *110*, 7566–7567.

(36) Kim, J. B.; Leonard, J. J.; Longo, F. R. *J. Am. Chem. Soc.* **1972**, *94*, 3986–3992.

(37) Gouterman, M. *J. Chem. Phys.* **1959**, *30*, 1139–1161.

(38) Spellane, P. J.; Gouterman, M.; Antipas, A.; Kim, S.; Liu, Y. C. *Inorg. Chem.* **1980**, *19*, 386–391.

(39) Marcus, R. A.; Sutin, N. *Biochim. Biophys. Acta* **1985**, *811*, 265–322.

(40) Leland, B. A.; Joran, A. D.; Felker, P. M.; Hopfield, J. J.; Zewail, A. H.; Dervan, P. B. *J. Phys. Chem.* **1985**, *89*, 5571–5573.

(41) Wasielewski, M. R. In *Photoinduced Electron Transfer, Part A-Conceptual Basis*, Fox, M. A., Chanon, M., Eds.; Elsevier: New York, 1988; pp 161–206.

(42) Silvers, S.; Tulinsky, A. *J. Am. Chem. Soc.* **1964**, *86*, 927–928.

(43) Walker, F. A.; Balke, V. L.; McDermott, G. A. *J. Am. Chem. Soc.* **1982**, *104*, 1569–1574.

(44) La Mar, G. N.; Eaton, G. R.; Holm, R. H.; Walker, F. A. *J. Am. Chem. Soc.* **1973**, *95*, 63–75.

(45) Weller, A. *Z. Phys. Chem. (Munich)* **1982**, *133*, 93–98.

(46) Application of the Born equation to a treatment of the energetics of solvation yields the following equation

$$\Delta G_{solv} = \frac{e_0^2}{2}\left(\frac{1}{r_+} + \frac{1}{r_-}\right)\left(\frac{1}{\epsilon} - \frac{1}{\epsilon_{ref}}\right) - \frac{e_0^2}{\epsilon a}$$

where r_+ is the radius of the donor, r_- is the radius of the acceptor, and a is the center-to-center distance of the solvated pair. This expression includes both the Coulomb energy change upon ion pair formation and the difference in free energy of ion solvation between the solvent in which the electrochemical potentials were measured (ϵ_{ref}) and the solvent in which the kinetics were measured (ϵ).

(47) Irvine, M. P.; Harrison, R. J.; Beddard, G. S.; Leighton, P.; Sanders, J. K. M. *Chem. Phys.* **1986**, *104*, 315–324.

(48) Schmidt, J. A.; Liu, J.-Y.; Bolton, J. R.; Archer, M. D.; Gadzekpo, V. P. Y. *J. Chem. Soc., Faraday Trans. 1* **1989**, *85*, 1027–1041.

(49) Rodriguez, J.; Kirmaier, C.; Johnson, M. R.; Friesner, R. A.; Holten, D.; Sessler, J. L. *J. Am. Chem. Soc.* **1991**, *113*, 1652–1659.